Supplementary Information

Aminophenol-formaldehyde particles containing hydrophilic benzenoid-amine for highly efficient solar-thermal water harvester

Rongtai Yu[a,b,*], Jianchao Xie[a], Fangfen Jin[a], Weiwei Lu[a], Mingzhu Jin[a], Xinyang He[a], Ashok K. Nanjundan,[b,c] Chengzhong Yu[b,*] and Xiaodan Huang[b,*]

[a] *School of Materials Science and Engineering, Jingdezhen Ceramic University, Jingdezhen, Jiangxi 333403, P. R. China*

[b] *Australian Institute for Bioengineering and Nanotechnology, The University of Queenslang, Brisbane, Queensland 4072, Australia.*

[c] *School of Engineering, University of Southern Queensland, Springfield, QLD 4300, Australia.*

* Corresponding authors, E-mail address: yurongtai@jci.edu.cn (R. Yu), c.yu@uq.edu.au (C. Yu), x.huang@uq.edu.au (X. Huang)

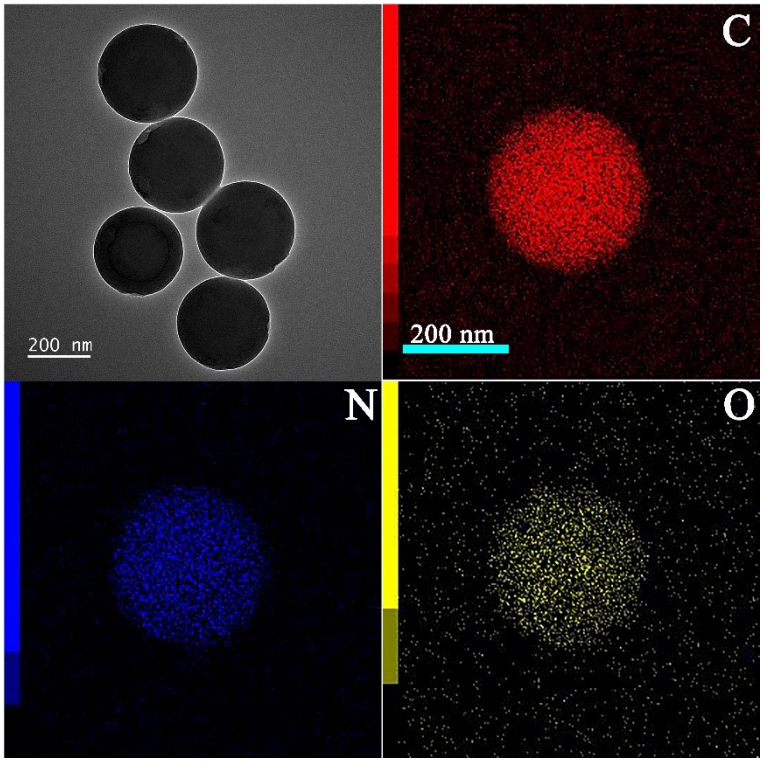

Fig. S1 TEM image and elemental mapping of the carbonized APF particles.

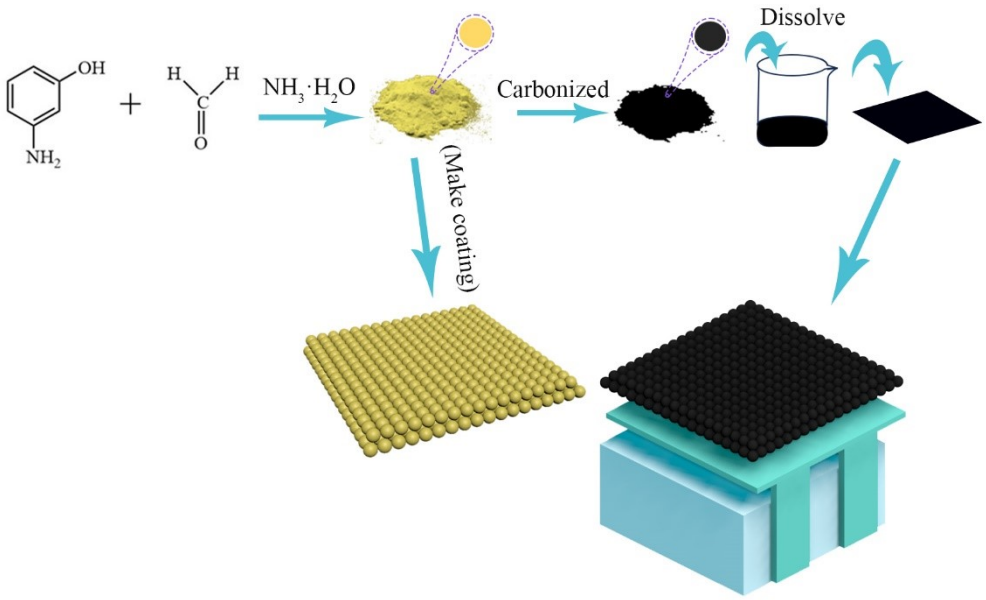

Fig. S2 The schematic diagram of the preparation process of the interface evaporator.

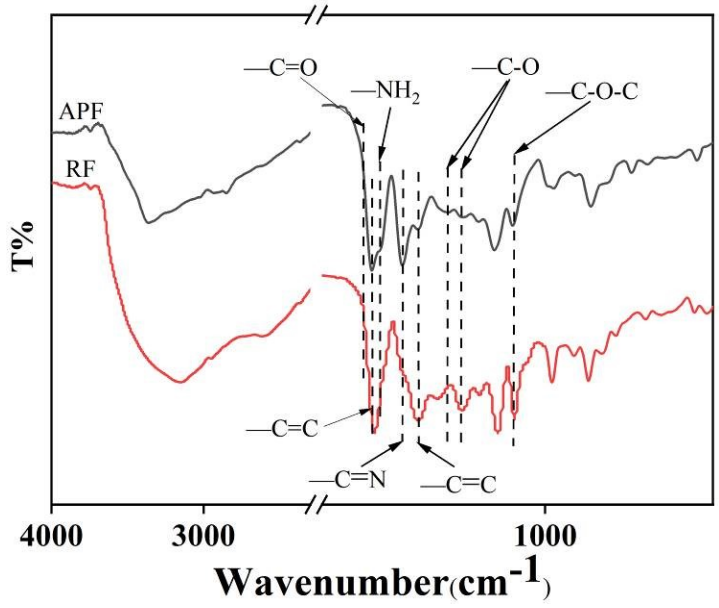

Fig. S3 FTIR spectra for APF and RF

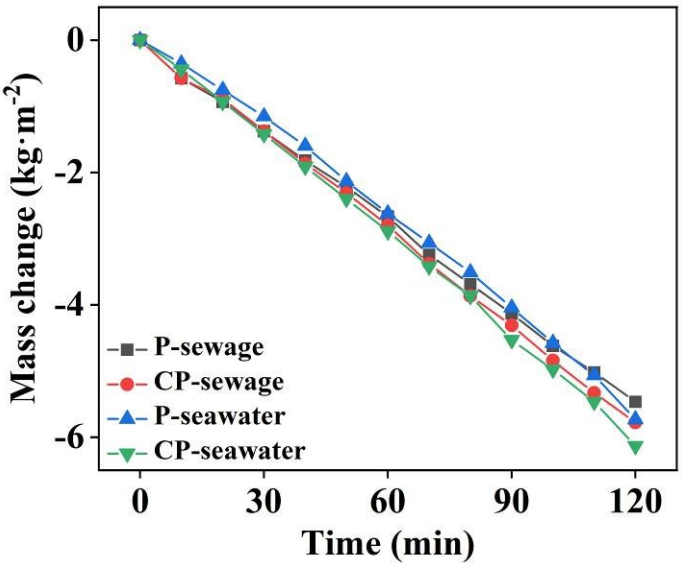

Fig. S4 The mass change of aminophenol-formaldehyde resins water evaporation performance under natural solar irradiance with functional time.

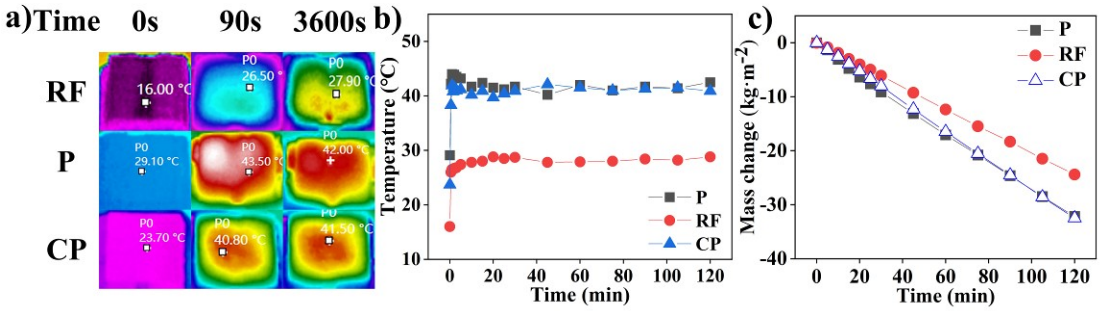

Fig. S5 The effect of hydrophilic benzenoid-amine on evaporation performance under a solar simulator. a) IR thermal images of the devices. b-c) Evaporation surface temperature and mass change as a functional time.

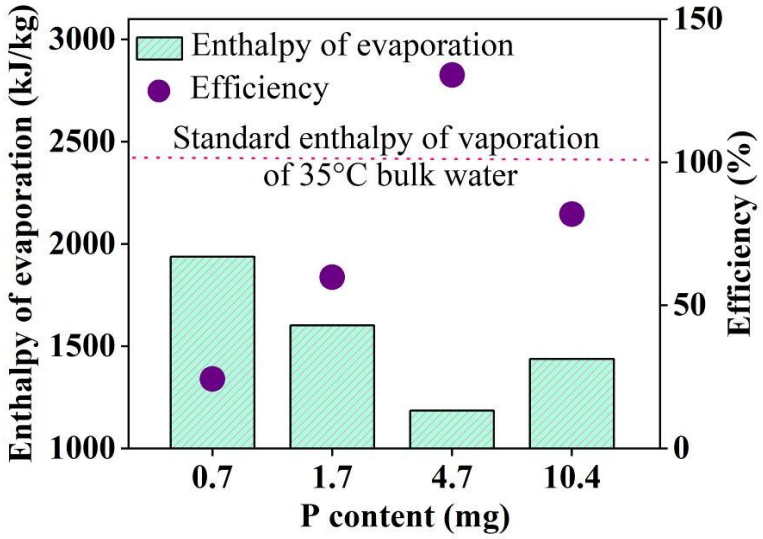

Fig. S6 The effect of the amount of polymer on the coating on evaporation enthalpy and evaporation rate under a solar simulator.

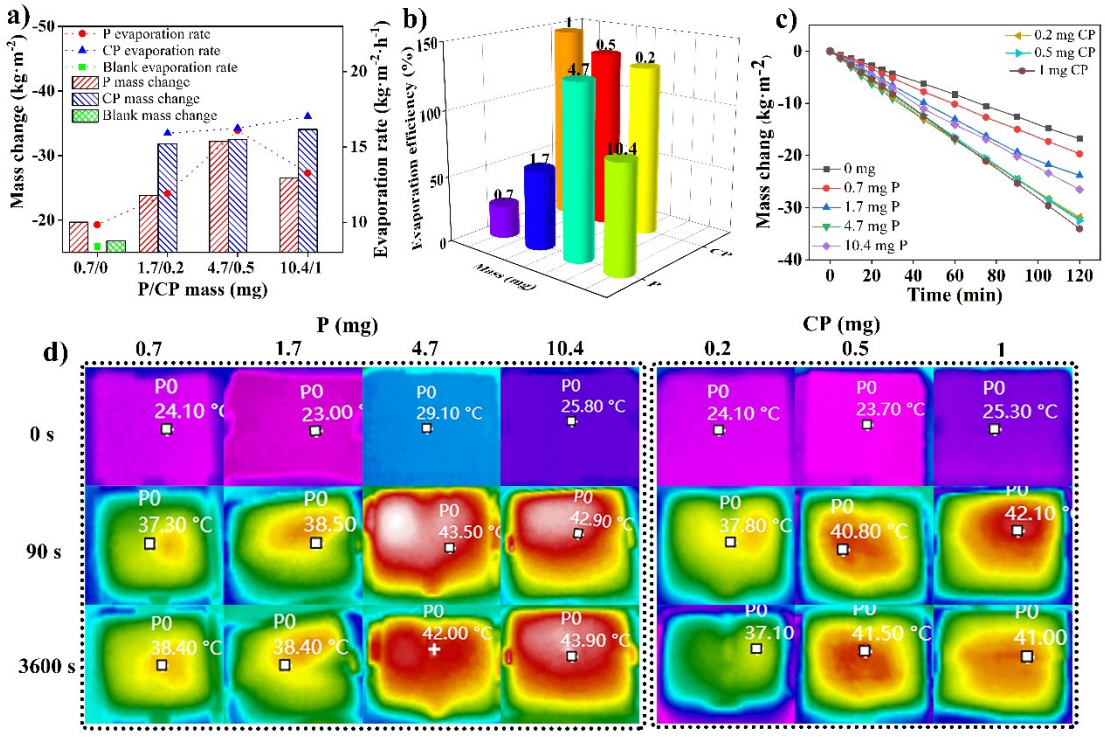

Fig. S7APF water evaporation performance under a solar simulator (3.9 kW m^{-2}, 15 A). a) The evaporation rates and mass change of water, b) evaporation efficiency, c) water mass change and d) IR images of evaporation surfaces during evaporation.

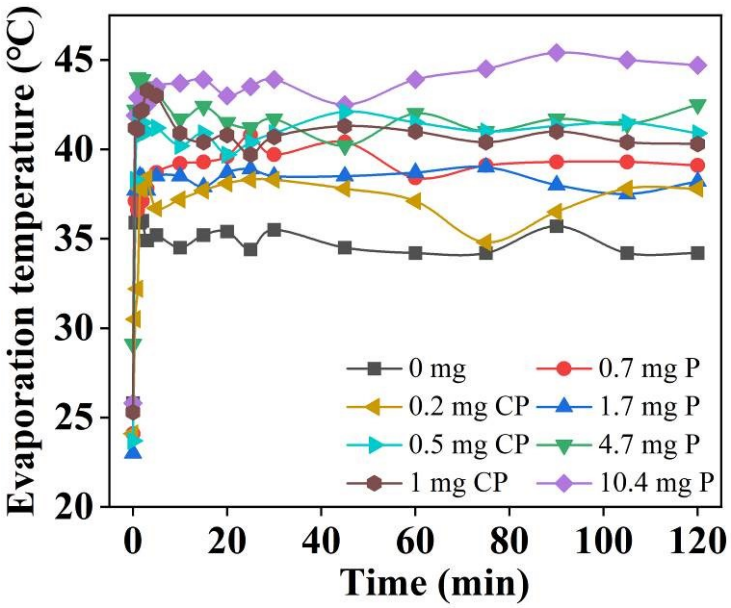

Fig. S8 Evaporation surface temperature of the APF-based evaporator with different P/CP weight.

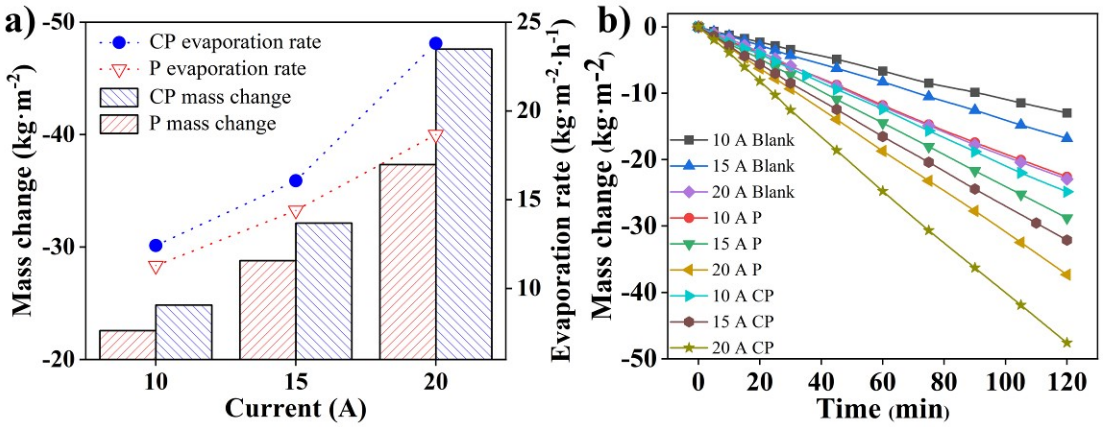

Fig. S9 The effect of light intensity on APF-based evaporator solar-to-vapor conversion performance in deionized water. a) Mass change and evaporation rate, b) water change as functional time.

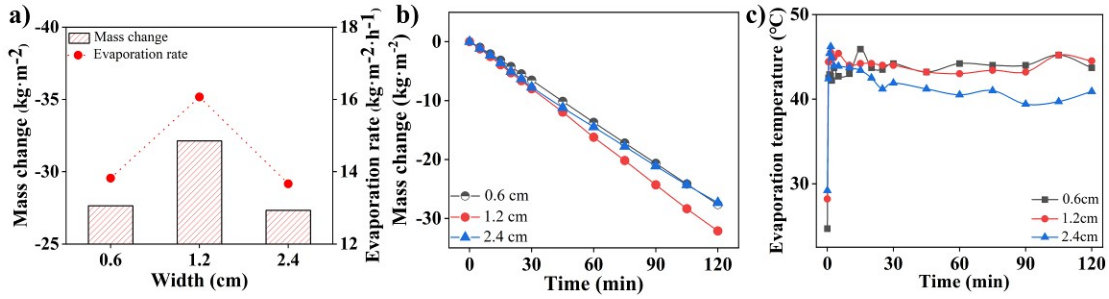

Fig. S10 The amount of water delivery on APF-based evaporator photothermal conversion performance (15 A). a) Mass change and evaporation rate. b) Mass change as functional time. c) Evaporation surface temperature as functional time.

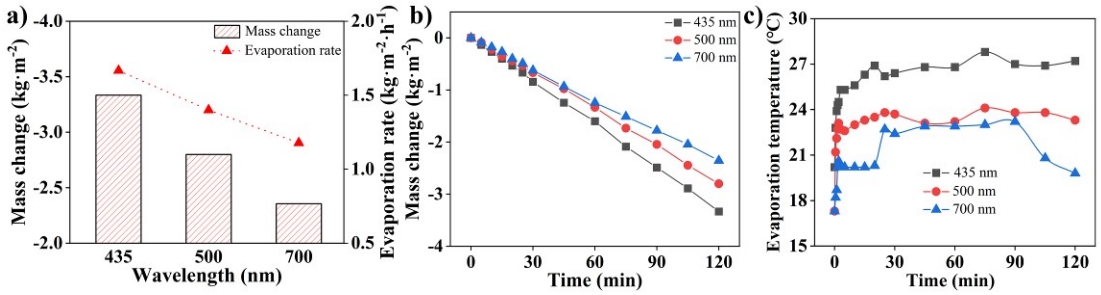

Fig. S11 The effect of monochromatic light on the photothermal conversion performance of APF-based evaporator. a) Mass change and evaporation rate. b) Mass change as functional time. c) Evaporation surface temperature as functional time.

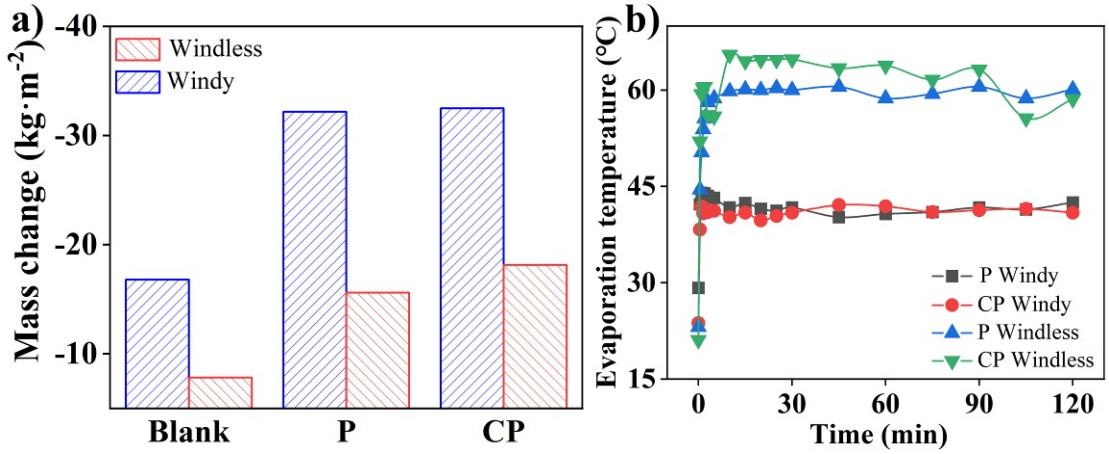

Fig. S12 The influence of wind at the exit of xenon lamp on APF-based evaporator photothermal conversion performance. a) Mass change and evaporation rate. b) Evaporation surface temperature as functional time.

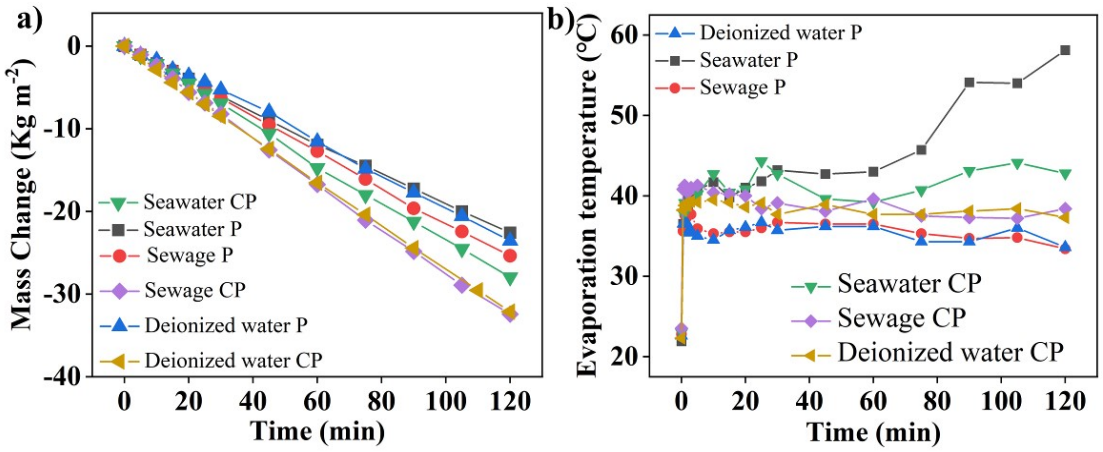

Fig. S13 Evaporation performance of APF-based evaporators in sewage, simulated seawater, and deionized water under laboratory test (3.9 kW m^{-2}). a) Mass change. b) Evaporation surface temperature.

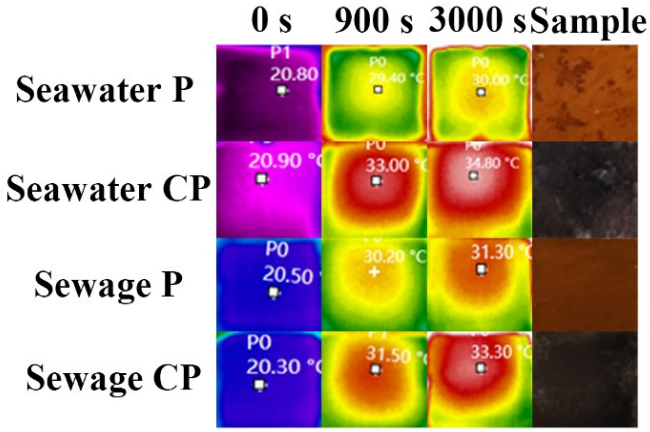

Fig. S14 IR images of the APF-based evaporator and the picture of the coating after the experiment.

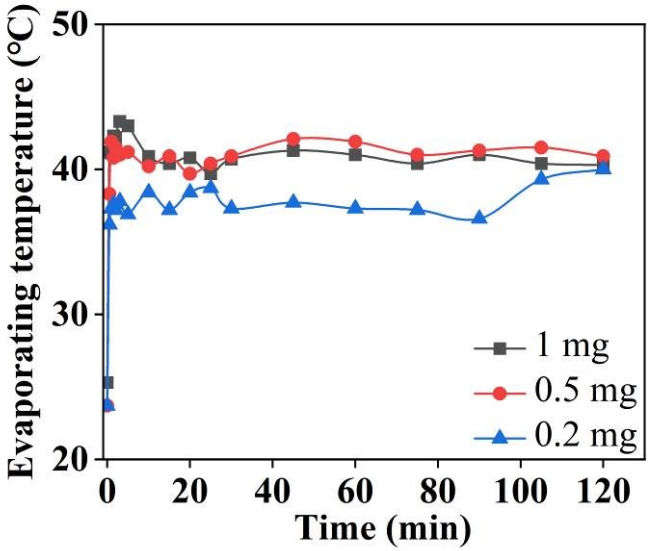

Fig. S15 Evaporation surface temperature of APF-based evaporator with different CP weight.

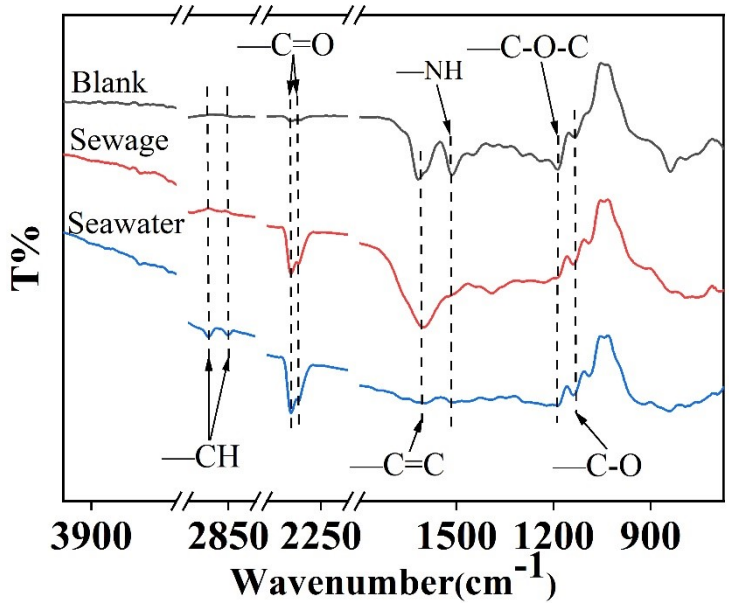

Fig. S16 FTIR of the carbonized APF-based evaporator after practical wastewater harvesting under laboratory test (3.9 kW m^{-2}).

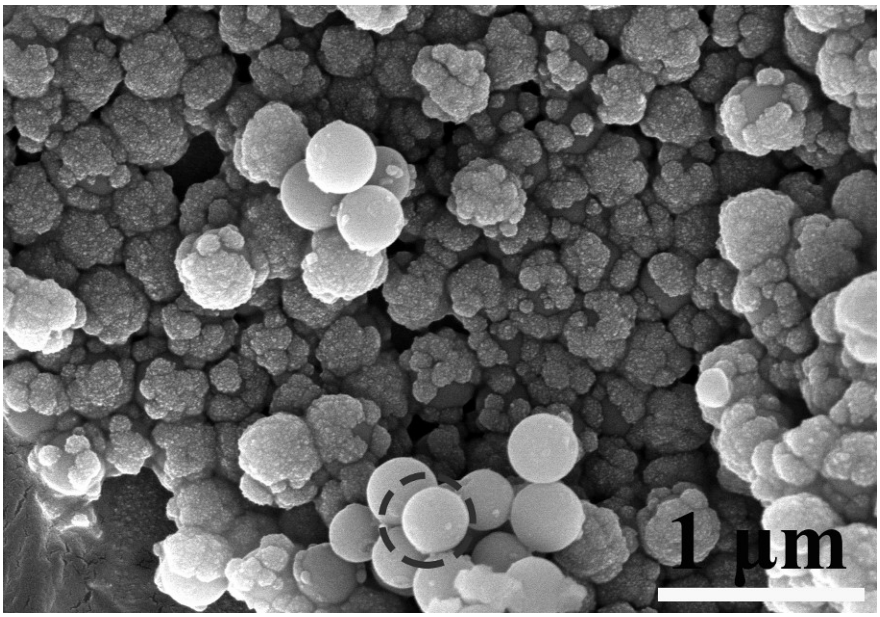

Fig. S17 The SEM image of carbonized APF-based evaporator after evaporation of sewage under laboratory test (3.9 kW m^{-2}).

Table S1 The element content analysis of the APF-based evaporator after evaporation of simulated seawater.

Element	Atomic	Conc, (wt.%)	Element	Atomic	Conc, (wt.%)
Mg	0.532	0.983	C	79.653	72.653
Ca	0.358	1.089	N	1.076	1.145
Na	1.069	1.866	O	16.480	20.024
Cl	0.832	2.240			

Table S2 The element content analysis of the carbonized polymer after evaporation of sewage.

The point of Fig S14			The point of Fig.5 f		
Element	Atomic	Conc, (wt.%)	Element	Atomic	Conc, (wt.%)
C	71.900	66.652	C	75.935	68.266
N	10.931	11.817	N	0.000	0.000
O	16.817	20.767	O	20.842	24.959
Si	0.352	0.763	Si	3.223	6.775